Applied Catalysis B: Environmental 142–143 (2013) 119–128

Contents lists available at SciVerse ScienceDirect

Applied Catalysis B: Environmental

journal homepage: www.elsevier.com/locate/apcatb

Facile template free method for textural property modulation that enhances adsorption and photocatalytic activity of aperiodic titania supported silica materials

Harrison S. Kibombo, Shivatharsiny Rasalingam, Ranjit T. Koodali*

Department of Chemistry, University of South Dakota, Vermillion, SD 57069, United States

ARTICLE INFO

Article history:
Received 5 February 2013
Received in revised form 1 May 2013
Accepted 10 May 2013
Available online 18 May 2013

Keywords:
Titania–silica
Hydrothermal
Porosity
Photodegradation
Rhodamine B

ABSTRACT

A series of aperiodic titania–silica photocatalysts were prepared in ethanolic solutions of co-solvents such as ethyl acetate (EtOAc), acetonitrile (ACN), acetone (ACT), and *N*,*N*′-dimethylformamide (DMF) using a combination of sol–gel chemistry and mild hydrothermal conditions. Extensive structural characterization emerged critical in demonstrating that the incorporation of such polar aprotic solvents is a viable approach for the enhancement and modulation of textural properties such as surface areas and pore sizes without the use of expensive templates. These studies revealed that the dark adsorption capacities of Rhodamine B (RhB) dye were dependent on the pore volume, and had minimal role on the photocatalytic degradation of the dye molecules. However, photocatalysts with large pore diameters exhibited improved initial degradation rates, suggesting that the sizes of the pores through which organics can diffuse in and out of the mesostructure are vital for their effective photocatalytic degradation under visible light irradiation. This work provides an insight into the use of facile preparation methods for the design of photocatalysts of desired porosities that are optimal for application in areas such as persistent organic pollutant remediation in waste water management.

1. Introduction

Increased mismanagement of wastewater from industrial processes exacerbates contamination and pollution of the ecosystem, and exposes living organisms to carcinogenic toxins, xenobiotics, biocides, and other organ disrupting agents [1–3]. Organic dyes are common components of effluents from such processes and have also emerged as persistent pollutants owing to their high chemical stability that is facilitated by the fused aromatic ring structures [4].

Conventional methods for the treatment of effluents such as coagulation–flocculation and precipitation, electrocoagulation, and ion-exchange are still limited by high energy costs, the use of expensive organic solvents, and uncontrollable sludge production. Other techniques such as physical adsorption are limited by mere transfer of the effluent from one phase to another (for *e.g.* adsorption of dye solution onto a solid matrix) incapable of degradation, and may require subsequent tertiary treatments thus rendering the remediation processes long and tedious. Such concerns present an urgent need for the creation of more cleanup programs composed of facile techniques that curb dye pollution in an efficient and economically sustainable approach.

More sustainable alternatives for wastewater treatment that have emerged in recent years are based on advanced oxidation processes (AOPs), such as ozonation, photocatalysis, photo-Fenton reaction, cavitation, and electrolysis [5]. AOPs are specifically designated for the removal of dissolved organics using highly reactive oxidative species (ROS) such as hydroxyl radicals that are believed to be primary actors in the degradation process [6,7]. These ROS are photogenerated under favorable semiconductor band-gap magnitudes that match or exceed the redox potential requirements [8]. Of the aforementioned technologies, heterogeneous semiconductor photocatalysis is an attractive option as it promises energy sustainability *via* the use of cheap light sources for the mineralization of highly refractory compounds such as organic dye pollutants, without the production of noxious by-products [9–11].

Titania based materials have proven to be the mainstay of recent research efforts owing to their high activity and low cost of production, for use in advanced oxidation processes such as the reduction of contaminants in order to provide clean drinking water [7,12,13]. In particular, an extensive review of aperiodic titania–silica (TiO_2–SiO_2) mixed oxides demonstrated their relevance and versatility in for environmental remediation [14]. Such mixed oxide photocatalysts have been explored for the degradation of methylene blue [15–17], methyl orange [18–20], and azo dyes [21] *etc.* The few existing literature reports employing such photocatalysts specifically for RhB dye degradation, implicate crystallinity

* Corresponding author. Tel.: +1 605 677 6189; fax: +1 605 677 6397.
E-mail addresses: Ranjit.Koodali@usd.edu, lktranjit@gmail.com (R.T. Koodali).

0926-3373/$ – see front matter © 2013 Elsevier B.V. All rights reserved.
http://dx.doi.org/10.1016/j.apcatb.2013.05.020

[22], sufficient exposure of active titania [23], high photoinduced charge carrier separation ability [24], and small anatase crystallite sizes [25]. Some literature reports purposely allude to the premise that the silica phase in the mixed oxide plays a significant role in increasing the adsorption capacity of organics [23,26,27], and improves the proximity between the organic substrate and the active sites (titania phase) thus facilitating their intimate interaction during the photocatalytic reaction [28–30]. However, such interactions need not necessarily imply improved photocatalytic activity, and some investigators have indeed indicated that adsorption is not always a pre-requisite for the photocatalytic reaction [31,32]. These existing studies, however, are limited by one or more of the following drawbacks: (1) the use of expensive surfactant templates for pore size and surface area expansion, (2) lack of detailed dark adsorption studies, (3) lack of a detailed and comprehensive physico-chemical characterization of the photocatalysts that preclude a clear understanding of structure-activity relationship that is essential for understanding dye degradation, (4) absence of studies pertaining to the role of polar aprotic solvents in the modulation of textural properties of mixed oxides, and (5) the misconstrued role of the silica phase that presumes that the higher activity of TiO_2–SiO_2 mixed oxides over TiO_2 is primarily due to the high adsorptivity of organics facilitated by the silica surface. Most vividly, the major drawback of existing literature is that the structure–activity relationships between the photocatalyst and dye degradation still remains unclear in the absence of a thorough characterization, and this work is a contribution to address these incongruences and provide much needed clarity.

The preparation of mixed oxide systems containing equimolar amounts of titania and silica that are used to degrade Rhodamine B (RhB) as a model xanthene cationic dye is detailed. Our studies revealed that the TiO_2–SiO_2 exhibited equilibrium adsorption capacities of RhB that are in some cases comparable to that of bare titania. However, the same photocatalysts demonstrate different photocatalytic performances indicating that properties responsible for catalytic activity are not governed by the adsorption. Thus, an optimal choice of the support and anatase loading is relevant for the minimization of radiation scattering by the "inert" phase and diffusion impediments in the porous structure that may limit the photocatalytic activity [33,34]. Specifically, catalysis practitioners that use porous materials have demonstrated that pore sizes are of significant influence on the resulting activity of TiO_2-based photocatalysts [35,36]. Enhanced activities appeared to be favored by the larger pore sizes [37,38] and in some cases, optimum average sizes were attained, beyond which the activities began to decline [39].

In this work, the TiO_2–SiO_2 photocatalysts were prepared using polar aprotic solvents including Drying Control Chemical Additives (DCCAs) such as acetonitrile and DMF that have proven essential for the production of crack free materials [40–42]. We recently demonstrated the applicability of polar protic co-solvents in tuning the crystallinity of such photocatalysts [43]. In contrast, polar aprotic solvents of varying dielectric constants and viscosities were chosen with care (ensuring dissolution in ethanolic TEOS), to alter the hydrolysis and condensation reactions that affect the resultant physico-chemical properties. The effect of polar aprotic solvents on the physico-chemical properties of TiO_2–SiO_2 is lacking in the literature. It is imperative to observe that the hydrolysis and condensation reactions are dependent on several competing factors that are not limited to the viscosity, degree of solvation, dielectric constants, boiling points, surface tension, and steric factors of the solvent media in the sol–gel reactions [44,45]. This article demonstrates that larger pores permit the diffusion of substrate molecules and products to access and leave the active sites most efficiently. The results provide practitioners in catalysis with fundamental information pertaining to the design of more improved low cost photocatalysts used in the areas of textile dye removal and the degradation of persistent organic pollutants (POPs).

2. Experimental

2.1. Materials and reagents

Commercially available titanium isopropoxide ($Ti[OPr^i]_4$, Acros, 98 + %), tetraethylorthosilicate, (TEOS, Fisher, 98%), ethanol (Pharmco-AAPER, ACS/USP grade, anhydrous), acetonitrile (Acros, ACS grade), *N*,*N*′-dimethylformamide (Acros, ACS grade), acetone (Pharmco-AAPER, ACS/USP grade), ethyl acetate (Fisher, ACS grade), conc. nitric acid (Acros, ACS grade), triethanolamine (TEA, (Acros, ACS grade), and isopropyl alcohol (IPA, Acros, ACS grade) were used as received. Ultrapure water (resistivity > 18 MΩ cm) was used throughout the experiments, and for the dilution of Rhodamine B (Alfa Aesar) to desired concentrations.

2.2. Preparation of photocatalysts

TiO_2–SiO_2 mixed oxide sols were prepared by simultaneous hydrolysis and condensation of alkoxide precursors, $Si(OC_2H_5)_4$ and $Ti[OCH(CH_3)_2]_4$, followed by hydrothermal treatment in order to accelerate the sol–gel reactions and induce crystallization. In a typical synthesis, 1.65 mL of $Si(OC_2H_5)_4$ was added slowly into a solution containing 9 mL of co-solvent that was dissolved in 9 mL of C_2H_5OH (200 Proof, anhydrous) under vigorous stirring in a Teflon liner. The hydrolysis process was initiated by the introduction of 1 mL of H_2O and the reaction was catalyzed by the addition of 100 μL of conc. HNO_3. $Ti(OCH(CH_3)_2)_4$ was added dropwise to ensure homogenous distribution and the suspension left to stir until gelation. Gelation was usually achieved in less than 3 h. The resultant gels were subjected to hydrothermal treatment in a Thermolyne autoclave reactor furnace and heated to a temperature of 120 °C for 14 h, filtered, and dried overnight at 70 °C. These powders were then ground and calcined in air at 500 °C for 6 h at a heating rate of 3 °C/min. in order to expel the organics. Thermogravimetric analyses, TGA (not shown) indicate that this calcination temperature and conditions were sufficient for the complete removal of solvent from the mixed oxide powder materials.

2.3. Characterization

The calcined samples were characterized by powder X-ray diffraction using a Rigaku Ultima IV with PDXL software. The diffraction patterns were recorded at room temperature employing Ni filtered Cu Kα radiation (λ = 0.15408 nm), an accelerating voltage of 40 kV, and emission current of 44 mA. The angle regions were scanned from 10° to 80° (2θ) with a step size of 0.02°. The textural properties such as specific surface area and pore size distribution of the mixed oxide materials were determined by using N_2 physisorption analysis. After the samples were dried overnight at 70 °C and degassed extensively at 100 °C, N_2 adsorption–desorption isotherms were obtained at −196 °C using a Surface Area and Pore Size Analyzer, NOVA 2200*e* (Quantachrome Instruments). The Brunauer–Emmett–Teller (BET) equation was applied within a relative pressure range (P/P_0) of 0.05–0.30 for the calculation of the specific surface areas. The pore volume was determined from the amount of nitrogen adsorbed at the highest relative pressure of $P/P_0 \sim 0.99$. The pore diameter and pore size distribution plots were obtained by applying the Barrett–Joyner–Halenda (BJH) model to the desorption isotherm. The UV–vis diffuse reflectance (DR) spectra of the samples were recorded in the range of 210–600 nm using a Cary 100 Bio UV–Vis spectrophotometer equipped with a Harrick DR praying mantis accessory. Transmission electron microscopy (TEM) images were recorded on a Tecnai G^2 instrument operating

at an accelerating voltage of 120 kV. The sample for TEM studies was prepared by suspending TiO_2–SiO_2 in ethanol and sonicating for 1 h. A drop of the suspension was cast on the copper grid mesh containing a carbon film, and allowed to dry overnight in a petri dish prior to collecting images. For additional structural information, the photocatalysts (prior to and after adsorption of RhB in the dark) were also dried in the oven overnight at 70–80 °C to eliminate moisture, and subsequent Fourier Transform-Infrared (FT-IR) spectroscopy studies were carried out. The spectra were collected in inert conditions (under N_2 flow) using OPUS 6.5 software operated using a Bruker instrument model ALPHA, and equipped with ATR diamond module of spectral range capabilities from 5000–500 cm^{-1}. Optimal spectra were obtained using 24 scans and 4 cm^{-1} resolution. A Malvern Nanosizer-90 was used for the measurement of ζ-potentials of the mixed oxide photocatalysts. For each experiment, an appropriate amount of photocatalyst was dispersed in aqueous 0.01 M KNO_3 solution to achieve a concentration of 1 mg mL^{-1}. The net charge on the photocatalyst was assessed by varying the pH in the range 2–11 using 0.1 M KOH and/or HNO_3. The results obtained were essential for postulating the mode of adsorption of RhB molecules on the photocatalyst surface.

2.4. Photocatalytic degradation experiments

The photocatalytic activity of the mixed oxide photocatalysts was assessed by monitoring the degradation of RhB dye in aqueous phase. 25 mg of photocatalyst was dissolved in 50 mL of dye solution (1×10^{-5} M) in a quartz cylindrical jacket reactor. The suspensions were stirred at a rate of 300 rpm in the dark for half an hour. The pH was detected in the range of 4–6 for all suspensions analyzed. The reaction temperature was maintained at 25 ± 2 °C by connecting the reactor to a water circulation bath. The photocatalytic reactions were carried out by irradiating the suspensions through a Pyrex glass cut filter ($\lambda > 400$ nm) for 6 h using a Xenon lamp (Newport 1000 W) as the light source. These experimental conditions were maintained throughout the course of the experiment. The light intensity in the reaction medium was estimated to be 92 mW cm^{-2} by placing the reactor 6 cm away from the light source. The intensity at back outer surface of reactor (without suspension), I_s = 113 mW; intensity at back outer surface of reactor (with suspension) I_{os} = 9.28 mW; and intensity of light in reaction medium $I_r = (I_s - I_{os})/\pi r^2$ = 91.7 mW cm^{-2}. During irradiation, 5 mL aliquots were drawn at selected time intervals for the kinetic studies, centrifuged at 4200 rpm for 30 min, and analyzed by UV–vis spectroscopy. The concentration of remnant RhB in solution was calculated using a calibration plot made previously, and by using the value of maximum absorbance from the spectra obtained at wavelength, λ_{max} = 554 nm. The photodegradation rates were calculated assuming pseudo-first order kinetics, and the apparent initial rate constant (k_0) was calculated from the first-order kinetic plot using the equation $\ln(C_t/C_0) = k_0 t$, where C_0 is the initial concentration of RhB and C_t is the concentration of RhB at time t = 60 min. During photocatalytic degradation, the formation of intermediates can interfere with the kinetics determination because of competitive adsorption and degradation. Thus, 60 min was used for calculation of apparent initial rate constant since pH changes and effect of intermediates can be considered to be negligible. It has been suggested that at low initial concentrations of dyes (millimolar and lower), use of first-order kinetic plot is appropriate. Such treatment of kinetic data has been recognized by Xu and Langford [33]. Our photocatalytic experiments indicate reproducibility of ~5%.

Additional experiments were carried in the presence of N_2 flow, isopropyl alcohol (IPA), and triethanolamine (TEA) in order to eliminate molecular O_2, and scavenge •OH radicals, and photogenerated holes (h^+) respectively, with intent to determine the active species that are playing a central role in RhB degradation under our experimental conditions. Experiments with IPA involved use of 2 mL of 500 mM to the photocatalyst suspension as described previously and irradiated under identical conditions. For experiments, involving TEA, 3.3 mL of 500 mM of TEA was added to the photocatalyst and irradiation carried out as described previously.

2.5. Adsorption experiments

Adsorption experiments were carried out using working solutions of concentrations from 1×10^{-5} M to 1.6×10^{-4} M of RhB. The adsorption were investigated by suspending 20 mg of photocatalyst in 20 mL of aqueous RhB in amber bottles, and subjected to the aforementioned conditions with the stirring time changed to 14 h prior to analysis. The equilibrium concentration of RhB solution after adsorption in the dark was calculated using the value of maximum absorbance obtained at wavelength (λ_{max} = 554 nm) from the UV–vis spectra. The equilibrium adsorption capacity q_e (mol g^{-1}) was calculated using: $q_e = ((C_o - C_e)V/m)$; where C_0 is the initial concentration of the RhB solution (M), C_e is the equilibrium concentration (M), V is the volume of the RhB solution (mL), and m is the adsorbent mass (mg).

3. Results and discussion

3.1. Powder XRD analysis

Powder X-ray diffraction (XRD) was carried out to investigate the phase composition of the photocatalysts and elucidate the impact of solvent choice on the crystal structure. Fig. 1A represents the XRD plot of bare TiO_2 (T-E) prepared in only ethanol solvent. It exhibits peaks that are typically attributed to the anatase phase [46]. The addition of silica to titania in equimolar amounts (TiO_2:SiO_2 = 1:1) and in the presence of only ethanol solvent to attain TS-E, resulted in the reduction in intensity and loss of diffraction contrast of the peaks due to titania, suggesting occlusion of the titania crystallites in the amorphous silica phase. A change in solvent system from ethanol to ethanolic solutions of polar aprotic solvents such as ethyl acetate (TS-EtOAc), acetone (TS-ACT), and *N*,*N*-dimethylformamide (TS-DMF) resulted in the loss of intensity of titania peaks in the long range. The broad peak around 25° coincides with the peak attributed to the silica phase, and is also an indication of amorphicity in the photocatalysts as depicted by the diffractograms in Fig. 1B. A slight increase in intensity of the broad feature is observed between 2θ = 50 and 80° for TiO_2–SiO_2 materials prepared using EtOAc, ACN, and DMF based. The crystallographic features suggest more amorphicity than that those prepared in ethanol only, and this may be due to the variation in hydrogen bonding properties of the DCCA that influence the hydrolysis rates of the metal alkoxides. When polar aprotic solvents such as *N*,*N*-DMF and CH_3CN are utilized, the $M(OR)_x$ groups are solvated to form $M(OR)_x$–DCCA solvate complexes. Because of the solvate formation, the alkoxides would be stable toward hydrolysis, limiting the attack of the nucleophile (water) to replace OR groups attached to metal atoms and result in longer gelation times. These solvents characteristically lack protons for H-boding to the hydroxyl groups and this has an effect of reducing the electrophilicity on the Si and Ti atoms, rendering the metal atoms (Si and Ti) less susceptible to nucleophilic attack by acid, and thus slowing down hydrolysis as a result [44,47]. It is also probable that these co-solvents form strong hydrogen bonding networks that effectively slows the condensation process [48]. This phenomenon becomes even more relevant when the electrophilicity of the metal is high such as in Ti-based alkoxides. The resultant TiO_2–SiO_2 materials are thus amorphous, and only show a characteristic SiO_2 peak in the powder diffraction

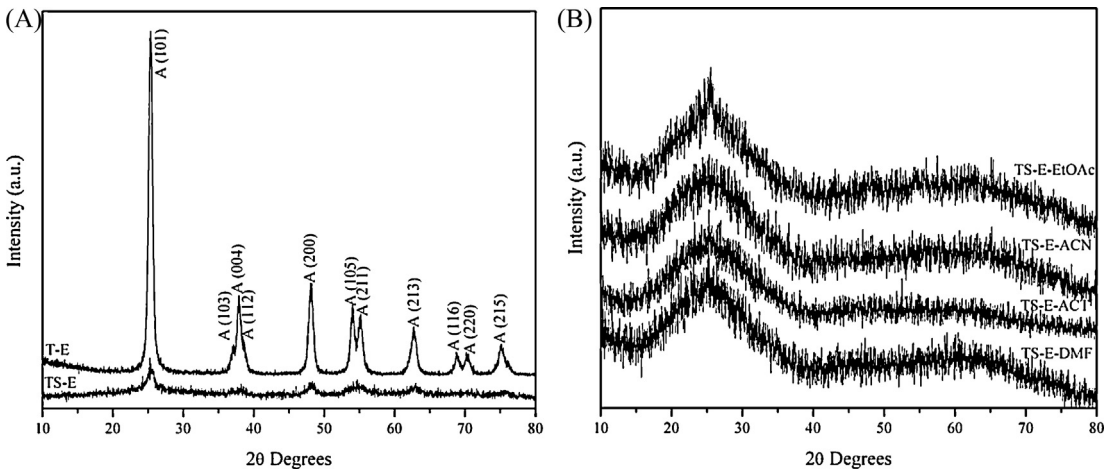

Fig. 1. Powder X-ray diffraction patterns exhibiting phase properties of (A) crystalline TiO_2 (T-E) and TiO_2–SiO_2 (TS-E) prepared using only ethanol, and (B) TiO_2–SiO_2 prepared using ethanolic solutions of ethyl acetate (TS-E–EtOAc), acetonitrile (TS-E–ACN), acetone (TS-E–ACT), and *N*,*N*′-dimethylformamide (TS-E–DMF) in equal v/v ratios.

data. The titania crystallites formed in the bulk are small (<3 nm), highly dispersed on the silica support, and thus not detected by powder XRD.

3.2. Bandgap determination

Bandgap energies for the photocatalysts prepared were estimated by extending the tangential lines to the abscissa of the Tauc plots $[F(R_\infty)E]^n$ *versus* E, where $n = ½$ for an indirect bandgap such as TiO_2, which were generated from UV–vis diffuse reflectance spectroscopy (DRS) plots transformed *via* the Kubelka–Munk function. The estimates derived from the Tauc plots in Fig. 2 suggest that the addition of silica phase is of minimal influence on the bandgap energies. The band gap of TiO_2 (T-E) and TiO_2–SiO_2 (TS-E) prepared with ethanol only as solvent appear invariable around 3.16 and 3.11 eV respectively. However the addition of polar aprotic solvents as co-solvents in the presence of ethanol results in an adjustment in the bandgap energies from 3.11 to 3.51, 3.55, 3.46, and 3.56 eV for TS-E–EtOAC, TS-E–ACN, TS-E–ACT, and TS-E–DMF respectively. It is likely that the addition of co-solvents leads to pore expansion as observed by an increase in surface area, and thus the surrounding silica restricts the growth in size of anatase crystallites. Similar effects due to silica addition have been reported previously [49,50] and the reduction in crystallize sizes is reflected in the increase in bandgap energies.

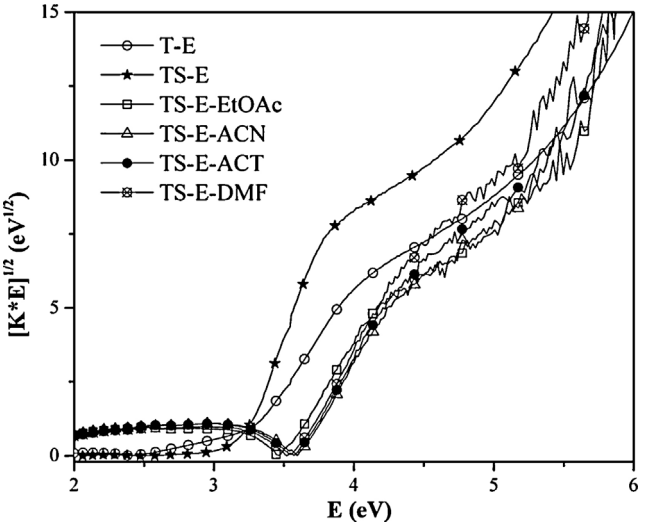

Fig. 2. Tauc plots used to estimate the band gap energies of crystalline TiO_2 (T-E) and TiO_2–SiO_2 (TS-E) prepared using only ethanol, compared to TiO_2–SiO_2 prepared using ethanolic solutions of ethyl acetate (TS-E–EtOAc), acetonitrile (TS-E–ACN), acetone (TS-E–ACT), and *N*,*N*-dimethylformamide (TS-E–DMF) in equal v/v ratios.

3.3. N_2 physisorption analysis

Surface area and pore size analysis was carried out to establish correlations from phenomenon derived from the nitrogen molecules that are physisorbed by these mixed oxide photocatalysts. Fig. 3A displays nitrogen isotherms of TiO_2, and TiO_2–SiO_2 prepared with ethanol only compared to those prepared in the presence of polar aprotic co-solvents. According to the IUPAC classification, TiO_2 (T-E) exhibited a type V sorption isotherm. In contrast, titania with a silica phase in the presence of ethanol solvent to form TiO_2–SiO_2 (TS-E) resulted in a change in the sorption isotherm to type IV. The characteristics of type IV materials are similar to that of type V with the exception that there is a modest increase in the amount of nitrogen adsorbed at low relative pressures in the type IV classified materials in comparison to type V that is relatively flat at low relative pressures. The increase in amount adsorbed may be due to lateral interactions between adsorbed molecules that are stronger than the interactions between the adsorbent surface and adsorbate [51]. Typically, filling and emptying of the pore with retention of the multilayer of adsorbate occur at different pressures, thus giving rise to adsorption–desorption hysteresis that is usually attributed to thermodynamic and/or network (pore connectivity) effects. All the materials prepared in this study exhibit isotherms classified as Type H3 hysteresis loops that achieve the saturation vapor pressure without leveling off prior thus suggesting materials of loose assemblages of plate like particles forming slit like pores [51].

The Barrett–Joyner–Halenda (BJH) method was used to obtain pore size distributions (PSD). Fig. 3B displays the BJH pore size distribution plots that exemplify the effect of the choice of solvent. T-E (TiO_2 only) exhibited pores of predominantly 6.5 nm, and the addition of silica phase results in a drop in pore diameter to about 3.8 nm. This may be due to occlusion of pores by silica. The pores in TS-E–EtOAC were predominant around 7.9 nm, and a change in co-solvent to acetonitrile, acetone, and DMF resulted in materials exhibited pores of *ca.* 1.9, 3.8, and 2.2 nm respectively. The results are summarized in Table 1. It is beyond the scope of this work to probe the reasons for the effect of co-solvent in tuning the pore sizes since the sol to gel transformation that involve hydrolysis and

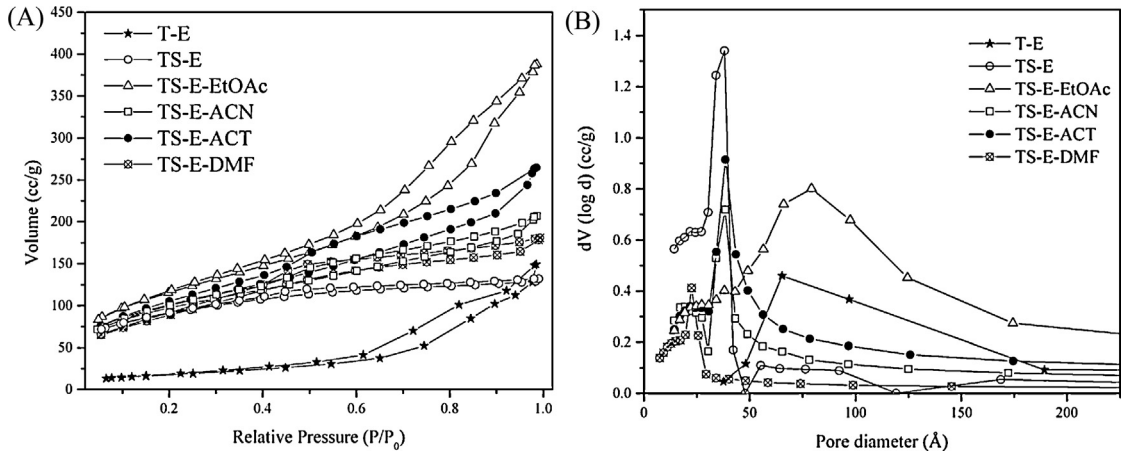

Fig. 3. A N_2 physisorption isotherms and (B) BJH pore size distribution plots of crystalline TiO_2 (T-E), TiO_2–SiO_2 (TS-E) prepared using only ethanol, TiO_2–SiO_2 prepared using ethanolic solutions of ethyl acetate (TS-E–EtOAc), acetonitrile (TS-E–ACN), acetone (TS-E–ACT), and *N*,*N*-dimethylformamide (TS-E–DMF) in equal v/v ratios.

condensation reactions are quite complex. As stated previously, these two reactions are dependent on competing factors such as degree of solvation of the alkoxides and viscosity, dielectric constants, boiling points, surface tension, of the solvent media.

Other aspects of the morphological features of the photocatalysts were investigated by employing electron microscopy to elucidate differences in the crystallographic properties.

3.4. TEM analysis

The pure titanium oxide and mixed oxide photocatalysts were compared and Fig. 4A is a high magnification image of TiO_2 exhibiting fringes indicative of anatase crystallites of about 8 nm in size. The lower magnification image in Fig. 4B shows agglomerated highly crystalline particles that result in peaks of high diffraction contrast in the powder XRD as discussed earlier. The TiO_2–SiO_2 photocatalyst prepared using ethanol and ethyl acetate co-solvent was used as a representative sample owing to its large pore sizes and enhanced photocatalytic activities. The high and low magnification images illustrated in Fig. 4C and D respectively indicate high porosities, and the occlusion of titania crystallites. The crystallite sizes of titania in the mixed oxides were indeterminate due to the high amorphicity as confirmed by broad features in the XRD plots.

3.5. Photocatalytic degradation of RhB

RhB is stable under visible light irradiation in the absence of photocatalysts. The concentration of remnant RhB in solution after visible light irradiation in the presence of TiO_2–SiO_2 photocatalyst was analyzed using UV–vis spectrophotometry. RhB molecules may adsorb on the surface of the photocatalyst through diethylamino or carboxylic groups, and the reduced peak intensity shown after dark condition depicts adsorption of some RhB molecules. The absorption peak position is maintained at λ_{max} = 554 nm similar to that of fresh RhB (1×10^{-5} M) as illustrated by the UV–vis absorption spectra in Fig. 5. The rate of degradation of RhB appears to be faster with TS-E–EtOAc than T-E (bare TiO_2) and the reasons are detailed later in this manuscript.

Under visible light irradiation ($\lambda > 420$ nm) and in the presence of a photocatalyst, RhB (and subsequently its degradation products) can absorb photons. The excited molecule thus transfers the LUMO electrons to the conductive band of TiO_2 where conductive electrons can react with pre-adsorbed oxygen molecules to produce reactive oxygen species (ROS) such as $O_2^{\bullet -}$, $^{\bullet}OOH$ and $^{\bullet}OH$. These ROS mainly attack the auxochromic groups and induce *N*-de-ethylation of the alkyl amine group [30]. It is also postulated that photogenerated holes (h^+) can degrade suspended unadsorbed RhB molecules and *N*-de-ethylated products that are released in solution [29]. In case of T-E, the absorption peak shows a blue shift with irradiation time and the peak maxima shifts progressively from 554 to 496 nm irradiation time until 4 h. Further irradiation leads to a decrease in the intensity of the peak at 496 nm (Fig. 5A). The peak position was invariable thereafter but the diminishing intensity suggests that the fused aromatic ring structures and dye chromophores were destroyed, and the decolorization observed was due to step-wise degradation processes and not due to photobleaching (TOC studies confirm the degradation of RhB). This behavior is also exhibited by titania–silica photocatalysts as

Table 1
Physisorption properties of TiO_2–SiO_2 mixed oxide materials showing the effect of porosities on adsorption and degradation of RhB dye molecules.

Photocatalyst	Solvent	Co-solvent	S_{BET}[a] ($m^2\,g^{-1}$)	BJH Pore diameter[b] (nm)	Bandgap energy (eV)	Pore volume ($mL\,g^{-1}$)	k_0[c] $\times 10^{-3}$ (min^{-1})	q_m[d] ($mg\,g^{-1}$)
T-E	Ethanol	–	76	6.5	3.16	0.22	9.12	9.58
TS-E	Ethanol	–	309	3.8	3.11	0.20	8.16	9.58
TS-E–EtOAc	Ethanol	EtOAc	412	7.9	3.51	0.60	11.0	28.7
TS-E–ACN	Ethanol	Acetonitrile	340	1.9	3.55	0.32	2.28	14.4
TS-E–ACT	Ethanol	Acetone	356	3.8	3.46	0.41	7.92	24.0
TS-E–DMF	Ethanol	DMF	325	2.2	3.56	0.28	5.16	9.58

The acronymns TS and E refer to titania–silica and ethanol respectively. EtOAc, ACN, ACT, and DMF denote ethyl acetate, acetonitrile, acetone, and *N*,*N*′-dimethylformamide polar protic solvents serving as co-solvents.

[a] BET is the Brunauer–Emmett–Teller equation applied to the adsorption isotherm that was used to determine the specific surface area.

[b] BJH is the Barrett–Joyner–Halenda method that was used to estimate the pore size distribution.

[c] k_0 is the initial apparent degradation rate constant after 60 min. of irradiation determined from $\ln(C_t/C_0) = kt$.

[d] q_m is the maximum adsorption capacity. The initial concentration of RhB dye was 1×10^{-5} M.

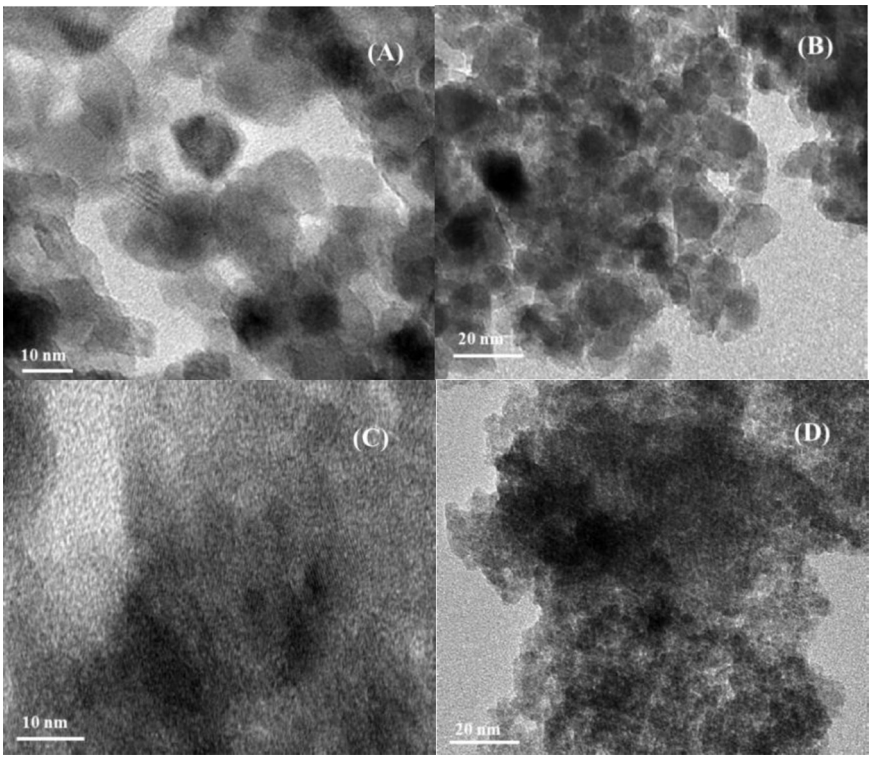

Fig. 4. TEM images showing the structural features of TiO_2 (T-E) control photocatalyst at (A) high magnification of 10 nm and (B) low magnification of 20 nm compared with (C) high magnification of 10 nm and (D) low magnification of 20 nm of TiO_2–SiO_2 mixed oxide prepared with an ethanol:ethyl acetate = 1:1 (TS-E–EtOAc) that demonstrated high pore sizes and photodegradation rate for RhB dye.

shown by one representative plot for TS-E–EtOAc in Fig. 5B. The hypsochromic (blue) shift observed is attributed to partial *N*-de-ethylation *via* visible light assisted photocatalysis. These shifts are due to the step-wise formation of *N*-de-ethylated intermediates of RhB, and studies pertaining to their identification by HPLC, LC–MS, and GC–MS are detailed elsewhere [52,53] and is not the focus of this work. Reaction kinetic studies were carried out to elucidate the factors contributing to the differences in degradation rate. The plots of (C_t/C_0) against time shown in Fig. 6 indicate a gradual loss in concentration of RhB due to degradation by the photocatalysts over 360 min of visible light irradiation. The initial kinetics are the main focus in this study and the inset of Fig. 6 suggests that RhB degradation by TiO_2–SiO_2 photocatalysts roughly follows pseudo-first order equation ($\ln(C_t/C_0) = k_0 t$) and the numerical values for apparent initial rate constant, k_0 (min^{-1}) are summarized in Table 1.

3.6. Influence of adsorption on photocatalytic performance

The causes for the differences in photodegradation efficiencies were investigated in order to establish a structure–activity relationship. The influence of adsorption has often been recognized in previous literature, and thus it is impetus to probe the adsorption of RhB on the TiO_2–SiO_2 photocatalysts.

The equilibrium sorption data were analyzed using Langmuir, Freundlich, and Redlich–Peterson isotherm Eqs. (1)–(3) using the non-linear method as shown in Fig. S1 in the Supporting Information section. The characteristic parameters were estimated for each

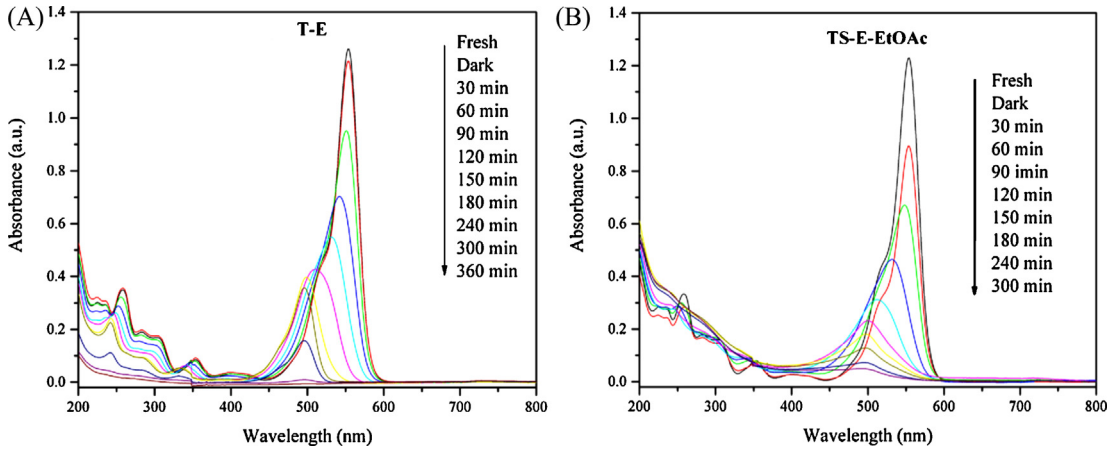

Fig. 5. Absorption spectra of RhB dye degraded under visible light irradiation for 6 h using (A) bare TiO_2 (T-E) and (B) a representative TiO_2–SiO_2 prepared with ethanol and ethyl acetate as co-solvent (TS-E–EtOAc).

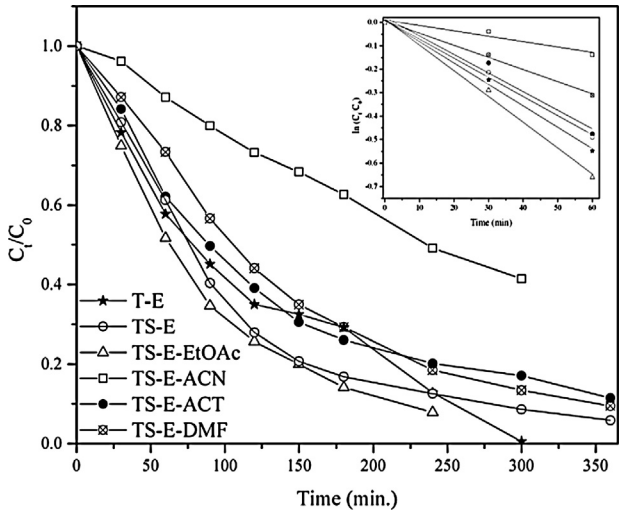

Fig. 6. Temporal course of photocatalytic degradation of 1×10^{-5} M RhB solution by TiO_2–SiO_2 mixed oxide photocatalysts under visible light irradiation ($\lambda > 420$ nm). Initial kinetics (60 min) of $\ln(C_t/C_0)$ plotted against time (min) are also shown in-set.

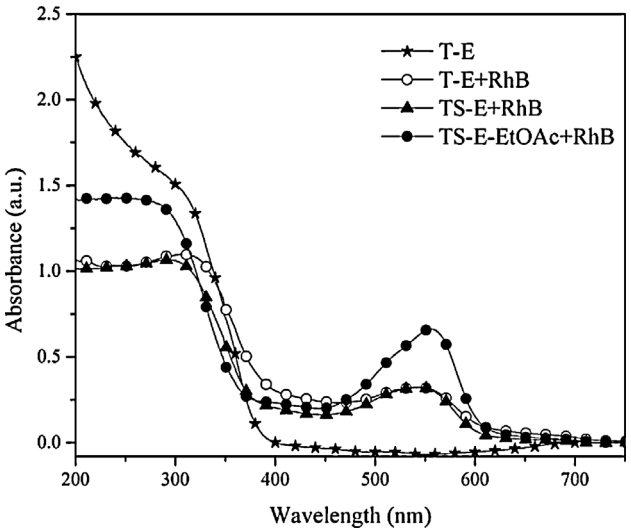

Fig. 7. Fourier Infrared spectra of bare photocatalysts and RhB dye molecules adsorbed on corresponding TiO_2 (T-E + RhB), and TiO_2–SiO_2 prepared in ethanol only (TS-E + RhB) and in the presence of ethyl acetate co-solvent (TS-E–EtOAc + RhB).

of the isotherms from equations adopted from previous published reports [54–56]:

$$q_e = \frac{q_m K_L C_e}{1 + K_L C_e} \quad \text{(Langmuir)} \tag{1}$$

$$q_e = K_F C_e^{(1/n)} \quad \text{(Freundlich)} \tag{2}$$

$$q_e = \frac{AC_e}{1 + BC_e^g} \quad \text{(Redlich} - \text{Peterson)} \tag{3}$$

q_e (mg g^{-1}) represents the dye adsorption capacities at equilibrium, q_m (mg g^{-1}) is the saturated monolayer sorption capacity, K_L (L mg^{-1}) is the Langmuir equilibrium constant that is related to adsorption free energy, and C_e (mg L^{-1}) is the equilibrium concentration of the dye in solution. n and K_F ((mg g^{-1})(L mg^{-1})$^{1/n}$) are Freundlich constants that indicate the adsorption intensity and the binding energy related to adsorption affinity respectively. A (L mg^{-1}), and B (L mg^{-1}) are the Redlich–Peterson constants and g, that typically lies between 0 and 1, is a measure of the extent of heterogeneity of the adsorption surface.

The data obtained from the adsorption isotherms are indicated in Table 2. The coefficients of determination (R^2) from the Langmuir isotherm model for T-E, TS-E, TS-E–ACN, and TS-E–DMF are 0.9781, 0.9156, 0.9213, and 0.9084 respectively. They are marginally higher than the R^2 values from the Redlich–Peterson model and noticeably higher than those exhibited by the Freundlich model. The only exception was sample, TS-E–EtOAc that showed smaller but similar R^2 values for the Langmuir isotherm in comparison to the Redlich–Peterson model. In addition, the g values of the Redlich–Peterson model from these afore-mentioned photocatalysts tend towards unity, thus suggesting an inclination to the Langmuir isotherm model as an appropriate fit for the adsorption data.

An interesting relationship between the saturated monolayer adsorption capacity (q_m), and the pore volume of the photocatalysts is observed and detailed in Table 1. TiO_2 (T-E) has a pore volume of 0.22 mL g^{-1} and exhibits q_m = 9.58 mg g^{-1}. The addition of a silica phase to form TiO_2–SiO_2 (TS-E) appears to be inconsequential on the pore volume and the adsorption capacity, maintaining values at 0.20 mL g^{-1} and 9.58 mg g^{-1} respectively. However, incorporating polar aprotic co-solvents such as DMF, acetonitrile, acetone, and ethyl acetate in the synthesis procedure results in photocatalysts of improved pore volumes of 0.28, 0.32, 0.41, and 0.60 cm^3 g^{-1} that exhibit values of q_m = 9.58, 14.4, 24.0, and 28.7 mg g^{-1} respectively. A larger pore volume (higher holding capacity) appears to facilitate access of RhB molecules into the pores and more adsorption capacities are achieved as a result. The other parameters obtained from the adsorption isotherm models employed are summarized in Table 2. The results indicate an absence of correlation between q_m and k_0 (apparent initial rate constant) and this could be attributed to a number of factors that include: (i) the viability of the degradation reactions taking place on the photocatalyst surface as well as in the bulk solution, (ii) the lack of sufficient adsorption sites to initiate the reaction, (iii) and/or the possibility of changes in the electronic properties of the photocatalyst surface and adsorption sites under visible light illumination [57].

The UV–vis diffuse reflectance spectra of the samples obtained after the adsorption of RhB (6×10^{-5} M) onto the photocatalysts are shown in Fig. 7. The absorption onset wavelength of bare TiO_2 (T-E) is in the range of 250–310 nm, with limited absorption in the visible range. A broad absorption is observed in the region of 470–630 nm, with a λ_{max} = 554 nm, and is indicative of the binding of RhB dye molecules onto the photocatalyst surface (T-E + RhB) that facilitates electron injection into the conduction band of the semiconductor. The addition of the silica phase to form TiO_2–SiO_2 (TS-E) and subsequent dye adsorption seems to exhibit a material (TS-E + RhB) whose diffuse reflectance pattern is similar to that of dye adsorbed on TiO_2. The porosities of TiO_2–SiO_2 can be modulated by using co-solvents such as ethyl acetate, and result in higher adsorption capacities as demonstrated by the plot for TS-E-EtOAC + RhB that shows a higher peak intensity than others. Thus, a high adsorption may imply that the photocatalyst has enhanced porosities and stronger binding interactions that facilitate higher adsorption of dye molecules.

The enhancement of RhB adsorption on TiO_2–SiO_2 may also be due to favorable surface interactions between the dye and the photocatalyst. Fig. 8 shows the electrophoretic mobility data that summarizes the zeta potential (ζ) as a function pH. The isoelectric point (IEP) of bare TiO_2 (T-E) was *ca.* 7.0 pH units, which is lower than the 4.7 and 4.9 pH units for TiO_2–SiO_2 photocatalysts *i.e.* TS-E and TE-E–EtOAC respectively. This change is consistent with the IEP results for silica based TiO_2 materials reported in previous literature [28,30,58–60]. The IEP for the other mixed oxide photocatalysts prepared in this study appeared in the range of 3–5 pH units and are not shown for the sake of clarity in Fig. 8. With respect to the

Table 2
Parameters of the Langmuir, Freundlich, and Redlich–Peterson adsorption isotherms derived from experimental data of adsorption of RhB on TiO_2–SiO_2 mixed oxide photocatalysts.

Photocatalyst	$k_0 \times 10^{-3}$ (min^{-1})	Langmuir			Freundlich			Redlich–Peterson			
		q_m ($mg\,g^{-1}$)	K_L ($L\,mg^{-1}$)	R^2	$1/n$	K_F	R^2	A ($L\,mg^{-1}$)	B ($L\,mg^{-1}$)^g	g	R^2
T-E	9.12	9.58	0.087	0.9781	2.498	0.0008	0.9168	0.022	0.089	0.99	0.9773
TS-E	8.16	9.58	0.100	0.9156	2.758	0.0004	0.8715	0.021	0.073	0.98	0.9130
TS-E–EtOAc	11.0	28.7	0.144	0.8571	2.337	0.0031	0.8616	0.165	0.024	0.75	0.8665
TS-E–ACN	2.28	14.4	0.030	0.9213	1.595	0.0062	0.8614	0.010	0.024	0.98	0.9198
TS-E–ACT	7.92	24.0	1.308	0.9508	2.504	0.0018	0.9519	0.116	0.031	0.78	0.9647
TS-E–DMF	5.16	9.58	0.083	0.9084	2.124	0.0016	0.8473	0.022	0.075	0.99	0.9073

The acronyms T, S, E, EtOAc, ACN, ACT and DMF refer to titania, silica, ethanol, ethylacetate, acetonitrile, acetone, and dimethylformamide respectively. The units for K_F are $(mg\,g^{-1})(L\,mg^{-1})^{1/n}$. k_0 is the initial apparent degradation rate constant after 60 min. of irradiation determined from $\ln(C_t/C_0) = kt$. q_m is the maximum adsorption capacity. The initial concentration of RhB dye was 1×10^{-5} M.

experimental conditions for the degradation of RhB in this study, our focus remains on the ζ-potential of the photocatalysts within the pH range of 6–7. The surface charge of TiO_2 appears to be slightly positive in this range and will thus induce an electrostatic interaction by binding with the negatively charged carboxylic ($-COO^-$) groups of the dye molecule. The RhB molecules are expected to have the carboxyl dissociated in the pH range of 6–7 according to previous reports [61,62]. Although the addition of a silica phase to TiO_2 to form TS-E lowers the IEP, the ζ-potential remains negative, thus inducing a binding mechanism that is alternative to that of bare TiO_2 and RhB. An electrostatic interaction between the negative charged mixed oxide surface with the positively charged diethylamino ($^+N(C_2H_5)_2$) groups of the dye molecule is proposed. This mechanism also applies to the co-solvent prepared photocatalysts such as, TS-E–EtOAc as indicated in Fig. 8 and all other titania–silica photocatalysts (not shown).

It has been suggested that the enhanced activity of TiO_2–SiO_2 mixed oxides in comparison to TiO_2 is due to the high adsorptivity of organics by the hydroxylated silica surface [32] and the role of surface hydroxyl groups have been implicated. FT-IR experiments were carried out in inert conditions (under N_2 flow) for all photocatalysts (before and after adsorption of RhB) in order to investigate the role of surface hydroxyl groups in varying the photocatalytic activities. Bands were observed in the FT-IR plot (Fig. 9) near 422, 933, and 1051 cm^{-1}, often ascribed to Si—O—Si bending [63], Ti—O—Si heterolinkages [64,65], and asymmetric Si—O—Si stretching [66] respectively in the titania–silica mixed oxides. The peaks at 1153 and 1212 cm^{-1} that appear in the RhB adsorbed on T-E + RhB photocatalyst may be attributed to C—N stretchings [67], which seem to be merged in the rest of the silica containing photocatalysts. The role of hydroxyl groups in the photocatalytic performance is disregarded owing to the minimal differences observed in the spectral region between 2700 and 3700 cm^{-1} alluded to —OH stretching due to fundamental vibrations of different surface hydroxyl groups and molecular water [65,68]. In addition, thermogravimetric analyses, TGA (not shown) indicated negligible difference (<3%) in weight losses that are typically attributed to the loss of physisorbed water and surface hydroxyl groups only and as such we believe that the surface OH density is somewhat similar. Such results were also observed by TGA–mass spectrometry studies for sol–gel titania based materials carried out by Pratsinis and co-workers [69].

Hence, we postulate that the factors contributing to catalytic activity span alternative parameters rather than surface hydroxyl groups. Also, it is worth mentioning that the crystallinities (and hence crystallite sizes) of the titania phase in the TiO_2–SiO_2 photocatalysts are similar and thus the differences in degradation performance is not due to this factor too in the present study. Similarly, the DRS spectra of all photocatalysts (excepting T-E and TS-E) are in a narrow range of 3.40–3.56 eV indicating that the particle sizes of titania are fairly similar.

The UV–vis studies of the RhB adsorbed samples and the zeta potential measurements provide useful information on the surface charge and binding mechanism; but they seem to be deficient in the elucidation to the differences in the degradation of the dye

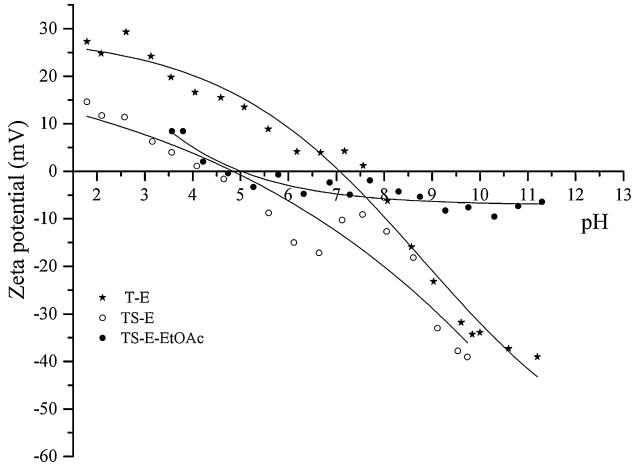

Fig. 8. UV–vis diffuse reflectance spectra of RhB dye molecules adsorbed on bare TiO_2 (T-E + RhB), and TiO_2-SiO_2 prepared in ethanol only (TS-E + RhB) and in the presence of ethyl acetate co-solvent (TS-E–EtOAc + RhB).

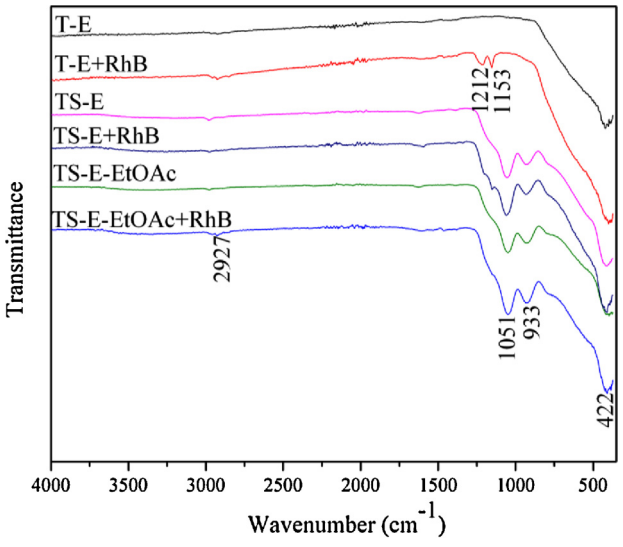

Fig. 9. ζ-potentials shown as a function of pH for RhB dye bare TiO_2 (T-E), and TiO_2–SiO_2 prepared in ethanol only (TS-E) and in the presence of ethyl acetate co-solvent (TS-E–EtOAc).

molecules. As indicated from XRD, DRS, and FT-IR studies, the titania–silica photocatalysts examined in this study have comparable crystallinities, particle sizes, and similar coverage of surface hydroxyl groups. The surface areas vary from 309 to 412 $m^2 g^{-1}$ and we do not see a correlation between the surface areas and the apparent rate constants (k_0). In focusing our attention on the pore sizes, we note that they seem to play an important role in affecting the photocatalytic activity. A trend that shows the dependence of dye degradation to the pore diameter is established. TS-E–EtOAc, TS-E, TS-E–ACT, TS-E–DMF, and TS-E–ACN exhibit initial apparent degradation rate constants, k_0 = 11.0, 8.16, 7.92, 5.16, and 2.28×10^{-3} min^{-1} due to pore diameters of 7.9, 6.5, 3.8, 3.8, 2.2, and 1.9 nm respectively. Similar observations were made for alumina supported titania materials in which the authors postulated the exchange of substrate molecules from pores or inert surface to the active centers as rate determining [31]. Consequently, our tabulated results indicate that the pseudo-first order apparent rate constant (k_0) is directly proportional to the BJH pore diameter of the materials. The larger pores are proposed to permit effective diffusion of reactant and products molecules to and from the active sites. We believe that there could be some reactions on the surface of the photocatalyst however minimal, and as such, access to the interior of the pores where most of the active sites are located, is critical for the degradation of RhB molecules. We observe that anatase TiO_2 (T-E) with a pore size of 6.5 nm and has an apparent rate constant of $k_0 = 9.12 \times 10^{-3}$ min^{-1} that is higher than some TiO_2–SiO_2 materials for RhB dye degradation after 60 min of visible light irradiation. The high activity of T-E in comparison to the photocatalyst, TS-E is due to its relatively large pore size and higher crystallinity even though the pore volume and the equilibrium amount of RhB adsorbed are similar (~0.2 mL g^{-1} and 9.58 mg g^{-1}) respectively.

The degradation of RhB has been investigated by carrying out scavenging experiments in order to elucidate the role of the reactive oxidation species (ROS). N_2 purged experiments were carried out to establish the role of molecular oxygen on the degradation of RhB. The process is known to occur *via* two competing processes *i.e.* de-methylation [70,71] and *N*-de-ethylation [72,73]. In order to compare the photocatalytic activity of titania with titania–silica materials, two photocatalysts, T-E, and TS-E–ACN were studied. After 2 h of irradiation, in the presence of oxygen (Fig. 6), ~65% of RhB was degraded in the presence of T-E photocatalyst. When the same experiment was carried out under N_2 purging, the activity was similar, *i.e.* 58% of RhB was degraded. This is indicated by a lower decrease in the absorbance maxima of RhB and a smaller hypsochromic shift in λ_{max} from 554 to 548 nm (Fig. S2A). Since the photocatalytic degradations are not totally ceased, $O_2^{\bullet -}$ radicals appear to be minor contributors to RhB degradation under our experimental conditions. A greater inhibition in the degradation was observed when using the silica based titania sample, TS-E–ACN photocatalyst. The amount of RhB degraded was estimated to be 55 and 33% respectively in the presence and absence of O_2.This result infers the importance of dissolved oxygen for photogenerated electron attack to form superoxide $O_2^{\bullet -}$ radicals that partake in the degradation processes in the titania–silica photocatalysts.

The presence of IPA (•OH scavenger) seems to increase the degradation of RhB on TiO_2 as depicted in Fig. S2C. After 2 h of irradiation, in the presence of IPA, ~90% of RhB was degraded using T-E photocatalyst. When the same experiment was carried out in the absence of IPA, 55% of RhB was degraded. Also, one notices that the absorption maxima is retained at 554 nm until 60 min of irradiation and shifts only slightly on further irradiation. This type of behavior has been previously attributed to the degradation of RhB *via* the action of •OOH [23]. The formation of •OOH can be rationalized by the following reactions as suggested previously [74].

$$(CH_3)_2CHOH + {}^{\bullet}OH \rightarrow (CH_3)_2C^{\bullet}OH + H_2O \quad (4)$$

$$(CH_3)_2C^{\bullet}OH + O_2 \rightarrow CH_3COCH_3 + {}^{\bullet}OOH \quad (5)$$

Thus, the enhanced degradation of RhB in the presence of IPA is attributed to the reaction of RhB with •OH and •OOH on TiO_2. However, the presence of IPA (•OH scavenger) seems to have negligible effect on the degradation of RhB on TiO_2–SiO_2 as depicted in Fig. S2D. After 2 h of irradiation, in the presence of IPA, ~48% of RhB was degraded in the presence of TS-E–ACN photocatalyst. When the same experiment was carried out in the absence of IPA, the activity was similar, *i.e.* 55% of RhB was degraded. This result indicates the less likelihood of •OH radicals to predominate in RhB degradation in our experimental conditions using titania–silica photocatalysts.

The presence of TEA (h^+ scavenger) provides a rather interesting result. In the presence of TEA, *N*-de-ethylation reaction is totally inhibited as depicted by the λ_{max} held at 554 nm (Fig. S2E) using bare TiO_2 (T-E) even after 2 h of irradiation. However, the steep decrease in absorption on illumination indicates degradation of RhB by de-methylation process as observed previously [71,75]. In contrast, as described previously, a shift in the absorbance maxima is observed using bare TiO_2 (T-E) in the absence of TEA until 4 h of irradiation. However, addition of silica to TiO_2 appears to totally impede the degradation of RhB as depicted by no change in the absorption peak intensity and no observable blue shift in λ_{max} after 2 h of visible light irradiation (Fig. S2F) is seen. This suggests that photogenerated holes (h^+) play a central role in the degradation of RhB by TiO_2–SiO_2 in our experimental conditions. Similar results that implicate photogenerated holes for RhB degradation are reported in the literature [76–78].

Thus, these photocatalytic experiments ultimately demonstrate promise for the use of such supported mixed oxide materials for the development of visible light active hybrid photocatalysts for environmental remediation. The ability to modulate the pore sizes is of significance in the diffusion and trapping of toxic organics within proximity to the active sites for effective degradation into biologically and chemically innocuous intermediates and by-products. Photogenerated holes (h^+) seem to be the most influential for RhB degradation using TiO_2–SiO_2 photocatalysts.

4. Conclusions

RhB degradation was demonstrated using TiO_2–SiO_2 mixed oxide materials under visible light irradiation. It was determined that the rate of degradation is dependent on the pore sizes, suggesting that the large pores are beneficial for the diffusion of RhB molecules to access and for the departure of degraded products from the active sites. The pore sizes appear to be of significance irrespective of the crystallinity, dispersion, surface areas, and adsorption properties of the photocatalysts. The adsorption capacities of the photocatalysts appear to be influenced by the pore volumes. It is imperative to develop photocatalysts with porosities that are optimum for adsorption and degradation of intended substrates.

Acknowledgements

We extend sincere gratitude to NSF-CHE-0619190, NSF-CHE-0722632, NSF-EPS-0903804, DE-EE0000270, and State of SD for funding this project.

Appendix A. Supplementary data

Supplementary data associated with this article can be found, in the online version, at http://dx.doi.org/10.1016/j.apcatb.2013.05.020.

References

[1] S.B. Grant, J.-D. Saphores, D.L. Feldman, A.J. Hamilton, T.D. Fletcher, P.L.M. Cook, M. Stewardson, B.F. Sanders, L.A. Levin, R.F. Ambrose, A. Deletic, R. Brown, S.C. Jiang, D. Rosso, W.J. Cooper, I. Marusic, Science 337 (2012) 681–686.
[2] X.-C. Jin, G.-Q. Liu, Z.-H. Xu, W.-Y. Tao, Applied Microbiology and Biotechnology 74 (2007) 239–243.
[3] J. Harris, A. McCartor, The World's Worst Toxic Pollution Problems Report 2011, Blacksmith Institute, 2011, pp. 1–76.
[4] Z. Carmen, S. Daniela, in: T. Puzyn (Ed.), Textile organic dyes–characteristics, polluting effects and separation/elimination procedures from industrial effluents–a critical overview, organic pollutants ten years after the stockholm convention – environmental and analytical update, InTech, 2012, pp. 1–33, ISBN: 978-953-307-917-2, InTech.
[5] C. Comninellis, A. Kapalka, S. Malato, S.A. Parsons, I. Poulios, D. Mantzavinos, Journal of Chemical Technology and Biotechnology 83 (2008) 769–776.
[6] M.R. Hoffmann, S.T. Martin, W. Choi, D.W. Bahnemann, Chemical Reviews 95 (1995) 69–96.
[7] M. Pelaez, N.T. Nolan, S.C. Pillai, M.K. Seery, P. Falaras, A.G. Kontos, P.S.M. Dunlop, J.W.J. Hamilton, J.A. Byrne, K. O'Shea, M.H. Entezari, D.D. Dionysiou, Applied Catalysis B: Environmental 125 (2012) 331–349.
[8] W. Choi, Catalysis Survey Asia 10 (2006) 16–28.
[9] M.N. Chong, B. Jin, C.W.K. Chow, C. Saint, Water Research 44 (2010) 2997–3027.
[10] M.A. Fox, M.T. Dulay, Chemical Reviews 93 (1993) 341–357.
[11] E. Grabowska, J. Reszczyńska, A. Zaleska, Water Research 46 (2012) 5453–5471.
[12] M. Shand, J.A. Anderson, Catalysis Science and Technology 3 (2013) 879–899.
[13] A. Di Paola, E. García-López, G. Marcì, L. Palmisano, Journal of Hazardous Materials 211–212 (2012) 3–29.
[14] H.S. Kibombo, R. Peng, S. Rasalingam, R.T. Koodali, Catalysis Science and Technology 2 (2012) 1737–1766.
[15] Z. Li, B. Hou, Y. Xu, D. Wu, Y. Sun, W. Hu, F. Deng, Journal of Solid State Chemistry 178 (2005) 1395–1405.
[16] K. Gude, V.M. Gun'ko, J.P. Blitz, Colloids and Surfaces A: Physicochemical and Engineering Aspects 325 (2008) 17–20.
[17] K. Shiba, S. Sato, M. Ogawa, Journal of Materials Chemistry 22 (2012) 9963–9969.
[18] X. Zhang, F. Zhang, K.-Y. Chan, Applied Catalysis A: General 284 (2005) 193–198.
[19] Y. Guo, S. Yang, X. Zhou, C. Lin, Y. Wang, W. Zhang, Journal of Nanomaterials 2011 (2011), Article ID: 296953.
[20] P. Cheng, M. Zheng, Y. Jin, Q. Huang, M. Gu, Materials Letters 57 (2003) 2989–2994.
[21] H. Chun, W. Yizhong, T. Hongxiao, Applied Catalysis B: Environmental 30 (2001) 277–285.
[22] Q. Zhang, D.Q. Lima, I. Lee, F. Zaera, M. Chi, Y. Yin, Angewandte Chemie International Edition 50 (2011) 7088–7092.
[23] P. Wilhelm, D. Stephan, Journal of Photochemistry and Photobiology A: Chemistry 185 (2007) 19–25.
[24] C. Kang, L. Jing, T. Guo, H. Cui, J. Zhou, H. Fu, The Journal of Physical Chemistry C 113 (2008) 1006–1013.
[25] F. Sayilkan, M. Asilturk, S. Sener, S. Erdemoglu, M. Erdemoglu, H. Sayilkan, Turkish Journal of Chemistry 31 (2007) 211–221.
[26] P.V. Messina, P.C. Schulz, Journal of Colloid and Interface Science 299 (2006) 305–320.
[27] J.B. Joo, Q. Zhang, I. Lee, M. Dahl, F. Zaera, Y. Yin, Advanced Functional Materials 22 (2012) 166–174.
[28] M.S. Vohra, K. Tanaka, Water Research 37 (2003) 3992–3996.
[29] X. Li, J. Ye, The Journal of Physical Chemistry C 111 (2007) 13109–13116.
[30] F. Chen, J. Zhao, H. Hidaka, International Journal of Photoenergy 5 (2003) 209–217.
[31] C. Minero, F. Catozzo, E. Pelizzetti, Langmuir 8 (1992) 481–486.
[32] C. Anderson, A.J. Bard, The Journal of Physical Chemistry 99 (1995) 9882–9885.
[33] Y. Xu, C.H. Langford, Langmuir 17 (2001) 897–902.
[34] J. Marugán, D. Hufschmidt, G. Sagawe, V. Selzer, D. Bahnemann, Water Research 40 (2006) 833–839.
[35] G.M. Walker, L.R. Weatherley, Chemical Engineering Journal 83 (2001) 201–206.
[36] U.G. Akpan, B.H. Hameed, Journal of Hazardous Materials 170 (2009) 520–529.
[37] S. Karcher, A. Kornmüller, M. Jekel, Dyes and Pigments 51 (2001) 111–125.
[38] Y. Zhao, M. Wei, J. Lu, Z.L. Wang, X. Duan, ACS Nano 3 (2009) 4009–4016.
[39] R. Yuan, R. Guan, J. Zheng, Scripta Materialia 52 (2005) 1329–1334.
[40] A. Parvathy Rao, A. Venkateswara Rao, Journal of Materials Synthesis and Processing 10 (2002) 7–16.
[41] R.F.S. Lenza, W.L. Vasconcelos, Journal of Non-Crystalline Solids 330 (2003) 216–225.
[42] K.T. Ranjit, K.J. Klabunde, Chemistry of Materials 17 (2004) 65–73.
[43] H.S. Kibombo, D. Zhao, A. Gonshorowski, S. Budhi, M.D. Koppang, R.T. Koodali, The Journal of Physical Chemistry C 115 (2011) 6126–6135.
[44] T.W. Zerda, G. Hoang, Chemistry of Materials 2 (1990) 372–376.
[45] M. Fukuoka, A. Makishima, Journal of the Ceramic Society of Japan 111 (2003) 0083–0086.
[46] T.P. Chou, Q. Zhang, B. Russo, G.E. Fryxell, G. Cao, The Journal of Physical Chemistry C 111 (2007) 6296–6302.
[47] C.J. Brinker, Journal of Non-Crystalline Solids 100 (1988) 31–50.
[48] I. Artaki, T.W. Zerda, J. Jonas, Journal of Non-Crystalline Solids 81 (1986) 381–395.
[49] V.S. Smitha, K.A. Manjumol, K.V. Baiju, S. Ghosh, P. Perumal, K.G.K. Warrier, Journal of Sol–Gel Science and Technology 54 (2010) 203–211.
[50] R.J. Davis, Z. Liu, Chemistry of Materials 9 (1997) 2311–2324.
[51] M. Kruk, M. Jaroniec, Chemistry of Materials 13 (2001) 3169–3183.
[52] C. Chen, W. Zhao, P. Lei, J. Zhao, N. Serpone, Chemistry – A European Journal 10 (2004) 1956–1965.
[53] Z. He, C. Sun, S. Yang, Y. Ding, H. He, Z. Wang, Journal of Hazardous Materials 162 (2009) 1477–1486.
[54] D.G. Kinniburgh, Environmental Science and Technology 20 (1986) 895–904.
[55] Y.S. Ho, Polish Journal of Environmental Studies 15 (2006) 81–86.
[56] S. Wang, Y. Boyjoo, A. Choueib, Z.H. Zhu, Water Research 39 (2005) 129–138.
[57] N. Guettaï, H. Ait Amar, Desalination 185 (2005) 439–448.
[58] N. Bao, Z. Wei, Z. Ma, F. Liu, G. Yin, Journal of Hazardous Materials 174 (2010) 129–136.
[59] S. Artkla, W. Kim, W. Choi, J. Wittayakun, Applied Catalysis B: Environmental 91 (2009) 157–164.
[60] J. Kiwi, M. Graetzel, The Journal of Physical Chemistry 91 (1987) 6673–6677.
[61] B.O. Haglund, L.-O. Sundelöf, S.M. Upadrashta, D.E. Wurster, Journal of Chemical Education 73 (1996) 889.
[62] K.H. Drexhage, Journal of Research of the National Bureau of Standards – A. Physics and Chemistry 80A (1976) 421–428.
[63] J. Xu, L. Li, Y. Yan, H. Wang, X. Wang, X. Fu, G. Li, Journal of Colloid and Interface Science 318 (2008) 29–34.
[64] J. Ren, Z. Li, S. Liu, Y. Xing, K. Xie, Catalysis Letters 124 (2008) 185–194.
[65] M. Galan-Fereres, L.J. Alemany, R. Mariscal, M.A. Banares, J.A. Anderson, J.L.G. Fierro, Chemistry of Materials 7 (1995) 1342–1348.
[66] P.J. Dirken, M.E. Smith, H.J. Whitfield, Journal of Physical Chemistry 99 (1995) 395–401.
[67] Z. Yu, S.S.C. Chuang, The Journal of Physical Chemistry C 111 (2007) 13813–13820.
[68] J. Ryczkowski, Catalysis Today 68 (2001) 263–381.
[69] R. Mueller, H.K. Kammler, K. Wegner, S.E. Pratsinis, Langmuir 19 (2002) 160–165.
[70] J. Li, X. Zhang, Z. Ai, F. Jia, L. Zhang, J. Lin, The Journal of Physical Chemistry C 111 (2007) 6832–6836.
[71] K. Yu, S. Yang, H. He, C. Sun, C. Gu, Y. Ju, The Journal of Physical Chemistry A 113 (2009) 10024–10032.
[72] J. Zhao, T. Wu, K. Wu, K. Oikawa, H. Hidaka, N. Serpone, Environmental Science and Technology 32 (1998) 2394–2400.
[73] T. Wu, G. Liu, J. Zhao, H. Hidaka, N. Serpone, The Journal of Physical Chemistry B 102 (1998) 5845–5851.
[74] P. Warneck, C. Wurzinger, The Journal of Physical Chemistry 92 (1988) 6278–6283.
[75] Z. He, S. Yang, Y. Ju, C. Sun, Journal of Environmental Sciences 21 (2009) 268–272.
[76] H. Fu, S. Zhang, T. Xu, Y. Zhu, J. Chen, Environmental Science and Technology 42 (2008) 2085–2091.
[77] S. Shamaila, A.K.L. Sajjad, F. Chen, J. Zhang, Journal of Colloid and Interface Science 356 (2011) 465–472.
[78] S. Shenawi-Khalil, V. Uvarov, S. Fronton, I. Popov, Y. Sasson, Applied Catalysis B: Environmental 117–118 (2012) 148–155.